OXFORD

SOT | Society of Toxicology
academic.oup.com/toxsci

Tox Spotlight article

TOXICOLOGICAL SCIENCES, 173(1), 2020, 65–76

doi: 10.1093/toxsci/kfz220
Advance Access Publication Date: October 18, 2019
Research Article

Tissue-Engineered Bone Tumor as a Reproducible Human *in Vitro* Model for Studies of Anticancer Drugs

Courtney Sakolish,[*] John S. House,[†] Alan Chramiec,[‡] Yizhong Liu,[*] Zunwei Chen ,[*] Susan P. Halligan,[‡] Gordana Vunjak-Novakovic,[‡,1] and Ivan Rusyn[*,1]

[*]Department of Veterinary Integrative Biosciences, Texas A&M University, College Station, Texas 77843; [†]Bioinformatics Research Center, North Carolina State University, Raleigh, North Carolina 27695; and [‡]Department of Biomedical Engineering, Columbia University, New York, New York 10032

[1]To whom correspondence should be addressed at Department of Biomedical Engineering, Columbia University, New York, NY 10032. Fax: (212) 305-4692. E-mail: gv2131@columbia.edu and Department of Veterinary Integrative Biosciences, Texas A&M University, College Station, TX 77843. Fax: (979) 847-8981. E-mail: irusyn@cvm.tamu.edu.

ABSTRACT

Studies of anticancer therapies in traditional cell culture models can demonstrate efficacy of direct-acting compounds but lack the 3-dimensional arrangement of the tumor cells and their tissue-specific microenvironments, both of which are important modulators of treatment effects *in vivo*. Bone cells reside in complex environments that regulate their fate and function. A bioengineered human bone-tumor model has been shown to provide a microphysiological niche for studies of cancer cell behavior. Here, we demonstrate successful transfer between 2 laboratories and utility of this model in efficacy studies using well-established chemotherapeutic agents. The bioengineered human bone-tumor model consisted of Ewing sarcoma (RD-ES) cancer cell aggregates infused into tissue-engineered bone that was grown from human mesenchymal stem cell-derived differentiated into osteoblasts within mineralized bone scaffolds. The tumor model was maintained in culture for over 5 weeks and subjected to clinically relevant doses of linsitinib, doxorubicin, cisplatin, methotrexate, vincristine, dexamethasone, or MAP (methotrexate, doxorubicin, and cisplatin combination). Drug administration cycles were designed to mimic clinical treatment regimens. The bioengineered tumors were evaluated days to weeks after the cessation of treatment to monitor the potential for relapse, using bioengineered bone and ES cell monolayers as controls. Drug binding to the scaffolds and media proteins and gene expression were also evaluated. We show that a bioengineered human bone tumor can be used as a microphysiological model for preclinical studies of anticancer drugs. We found that anticancer efficacy was achieved at concentrations approximating the human C_{max}, in contrast to traditional ES cell monolayers. These studies show that the bone-tumor model can be successfully transferred between laboratories and has predictive power in preclinical studies. The effects of drugs on the bone tumors and healthy bone were studied in parallel, in support of the utility of this model for identification of new therapeutic targets.

Key words: tissue chip; alternatives to animal testing < *in vitro* and alternatives; toxicogenomics < methods; safety evaluation; bone < systems toxicology.

Skeletal bone is a common target for metastasis of primary tumors formed in other tissues, including breast, lung, kidney, prostate, and thyroid (Ferguson and Turner, 2018), as well as to osteosarcoma and Ewing sarcoma (ES) that originate in bone. Ewing sarcoma is the second most common primary malignant bone tumor and is most frequently observed in adolescents in their second decade of life (Moore and Haydon, 2014). Although believed to arise from transformed bone marrow mesenchymal stem cells, ES tumors are histologically heterogeneous, with varying degrees of neural differentiation, and because they

grow rapidly and aggressively are prone to metastases and recurrence (Ferguson and Turner, 2018). Current treatment options include chemotherapy (vincristine, doxorubicin, cyclophosphamide, ifosfamide, and etoposide), surgery, and radiation; newer therapeutic modalities for ES are directed at targeting mTOR (a tyrosine kinase) and the fusion protein EWS-FLI1, and at using immunotherapy (Yu *et al.*, 2017). Despite advances in clinical outcomes using combination local therapy and chemotherapy, the long term cure rates remain at 20–30% for patients with metastasis at diagnosis (Khanna *et al.*, 2017). Mice are the most common model for studies of drug efficacy in ES, by injection of murine (allograft) or human (xenograft) tumor cells into the bone (Jacques *et al.*, 2019); however, these models are not without significant limitations such as limited throughput and scalability, as well as the lack of a human microenvironment and of the precise manipulation of the model needed to answer biological questions. Furthermore, to date there are no genetically engineered mouse models of ES, severely limiting the progress of the field (Jacques *et al.*, 2018).

As an alternative to animal models, *in vitro* cell culture is widely used, although it fails to model the complex *in vivo* microenvironment that recapitulates the native niche of solid tumors (Ronaldson-Bouchard and Vunjak-Novakovic, 2018). More recently, bone tumors have been bioengineered and studied *in vitro*, using human cancer cells and biomaterial scaffolds. Organ-on-a-chip models now seek to generate higher biological fidelity than traditional cell culture, using engineering approaches that yield functional tissue units capable of predicting organ-level responses (Marx *et al.*, 2016). Indeed, tissue-engineered tumor models are being grown *in vitro* to mimic actual human tumors. Recently, we established a protocol for bioengineering ES, by infusing tumor cell aggregates into humanized bone scaffolds engineered from bone marrow-derived mesenchymal stem cells. This allows for crosstalk between the tumor cells and osteoblasts in the tissue microenvironment, including secreted factors that mediate tumor growth and metastasis (Marturano-Kruik *et al.*, 2016). This novel *in vitro* model of ES is based on tumor cell growth within the tumor microenvironment (Chramiec and Vunjak-Novakovic, 2019). By utilizing both approaches within 1 model, this bone-tumor tissue chip was able to reestablish key properties of both native human tumors themselves (such as re-expression of cancer-related genes like STAT3 and presentation of a necrotic core), as well as properties related to their interaction with their bone niche, namely upregulation of focal adhesion genes, regeneration of a hypoxic and glycolytic phenotype, and recapitulation of angiogenic ability and vasculogenic mimicry (Villasante *et al.*, 2014). Critically for pharmacological investigations, our bone-tumor model can be maintained for prolonged periods (weeks to months), unlike the 2-dimensional *in vitro* cell culture models.

Some of our more recent studies have shown that biophysical stimuli mimicking those normally present within the native bone-tumor microenvironment resulted in the shift of tumor cells cultured in 3-dimensional settings toward a more native tumor phenotype (Marturano-Kruik *et al.*, 2015). In addition, we reported that therapeutic reagents with demonstrated efficacy in ES treatment, such as zoledronic acid, inhibited bone resorption mediated by osteoclasts (Villasante *et al.*, 2017). In this study, we aimed to evaluate the utility of our bioengineered human ES tumor model for a preclinical drug-screening paradigm. We tested whether a model that allows both crosstalk between cancer cells and replicates the key components of the bone-tumor microenvironment can provide valuable information about anticancer drug efficacy not detected using traditional *in vitro* models. The experiments included testing the reproducibility of this model across 2 laboratories in a series of independent experiments of dose-dependent effects of chemotherapeutic drugs, thereby addressing the critical issue of technology transfer necessary to promote the adoption of these models (Ewart *et al.*, 2017). We also compared this 3-dimensional model to the traditional monolayer culture of ES cancer cells using a number of cytotoxic drugs that are used in the clinic.

MATERIALS AND METHODS

Tissue-engineered bone and bone tumors. The 3D-B (3D-Bone) and 3D-B/T (3D-Bone Tumor) were grown at Columbia University as previously described (Grayson *et al.*, 2010; Marcos-Campos *et al.*, 2012; Villasante *et al.*, 2014), then shipped to Texas A&M University for testing. Cell culture scaffolds ($8 \times 4 \times 1$ mm) were prepared from decellularized bovine bone. Briefly, thick slices (~1.5 inches) of trabecular bone were obtained from the metatarsal of a bovine calf using a band saw. From these slices, a CNC milling machine was used to acquire rectangular bone cores with a cross-section of 4×8 mm, after which an IsoMetTM low speed wafering saw (Buehler, Lake Bluff, Illinois) was used to precisely cut 1 mm thick bone scaffolds. The scaffolds were washed in 0.5% SDS buffer to remove bovine cellular debris and subsequently treated with a DNase and RNase solution (Sigma-Aldrich, St Louis, Missouri) to remove bovine nuclear contaminants. The scaffolds were then lyophilized and measured individually for weight to determine whether they were within the ideal bone density range (11–18 mg) as previously shown (Grayson *et al.*, 2010).

Each scaffold was seeded with 1×10^6 primary human bone marrow-derived mesenchymal stem cells (hMSC) that were determined to express markers CD29, CD44, CD105, and CD166, and to not express CD14, CD34, and CD45 (Lonza, Basel, Switzerland). After 4 weeks of osteogenic differentiation of MSCs on osteoinductive scaffolds, the resulting engineered bone was either maintained in culture (3D-B) or infused with green fluorescent protein luciferase transduced Ewing sarcoma cells (RD-ES and ATCC) cultured as 3×10^5 cell spheroids, embedding 3 spheroids per scaffold. For 2-dimensional comparison, ES cells were cultured in a monolayer within a 96-well tissue culture plate (2D-T). All bioengineered tumors were cultured in RPMI-1640 medium (ATCC, Manassas, Virginia) supplemented with 10% FBS (Atlanta Biologicals, Flowery Branch, Georgia), and 1% pen-strep.

Upon receipt at Texas A&M University, the cultured tumors were placed into a custom 12-well polycarbonate plate and held suspended in place. Medium was changed daily for 1 week prior to testing, to allow for tissue equilibration after shipping. After this period, the vehicles alone (0.1% dimethyl sulfoxide [DMSO]) or drugs (linsitinib [12 μM], doxorubicin [4.16 μM], cisplatin [3, 10, 30 μM], methotrexate [0.1, 1, 10 μM], vincristine [0.1, 1, 10 μM], dexamethasone [0.1, 1, 10 μM], or MAP, a combination of cisplatin [4.4 or 44 μM], methotrexate [0.18 or 1.8 μM], and doxorubicin [0.1 or 1 μM]) were added into the culture medium (Figure 1). Medium was replaced completely on treatment days and at 50% on "rest days." Media samples were collected daily throughout the testing duration.

Analytical methods. Media samples containing linsitinib, doxorubicin, methotrexate, vincristine, and dexamethasone were analyzed by triple-quadrupole mass spectrometry (Agilent 6470, Santa Clara, California) coupled to high performance liquid chromatography (HPLC QqQ MS; Agilent 6470 MS 1290 Infinity II

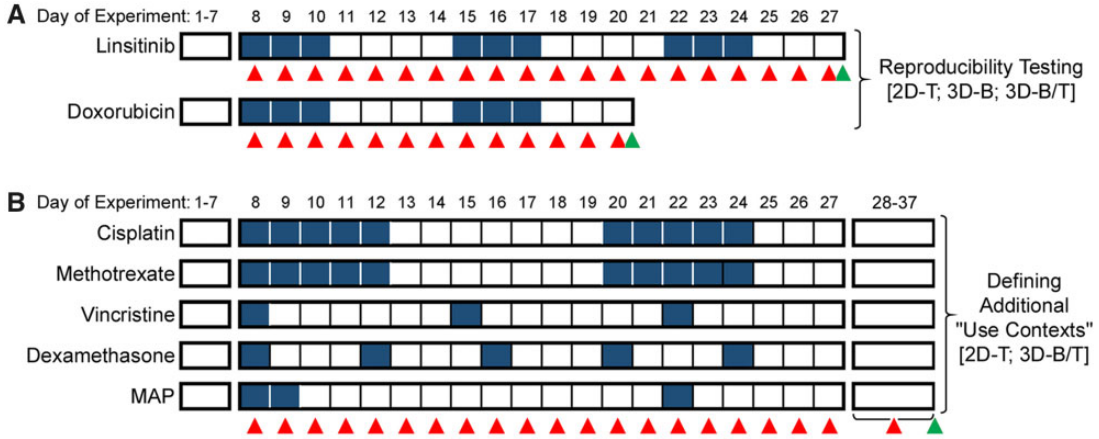

Figure 1. Experimental design. 3-dimensional bone, 3-dimensional bone-tumor, and 2-dimensional Ewing sarcoma cell monolayers were studied. A, Reproducibility testing. B, Drug studies. Treatments shown in each panel and concentrations for each drug are explained in Materials and Methods. Experimental schedule is shown with treatment days are shaded in blue. Days 1–7 and 28–37 (B) are not drawn to scale. Triangles show experimental days when cell culture medium was collected. Right-most triangle indicates the time point for formalin fixation and imaging, cell viability testing, or mRNA isolation. Abbreviations: 2D-T, 2D Ewing sarcoma cell monolayers; 3D-B, 3D bone; 3D-B/T, 3D bone-tumor.

HPLC) equipped with ZORBAX Eclipse Plus C18 guard and analytical columns (guard: 5 μm 20 × 2.1 mm; analytical: 1.8 μm, 100 Å 3.0 × 50 mm). The solvent gradient was based on the manufacturer's recommendations. Briefly, the column compartment was held at 40°C during sample analyses. The samples (10 μL each) were spiked with an internal standard and injected. The mobile phase flow rate was 0.4 mL/min, and the mobile phases were A: water with 0.1% (v/v) formic acid and B: acetonitrile with 0.1% (v/v) formic acid. The gradient was set to 90% A from 0 to 3 min, 5% A from 3 to 7 min, and 90% A from 7 to 10 min for column equilibration. Internal standards were neratinib (for linsitinib), ranitidine (for doxorubicin) (Abdel-Hamid and Sharma, 2004), aminopterin (for methotrexate) (Rodin *et al.*, 2013), vinblastine (for vincristine) (Guilhaumou *et al.*, 2010), and testosterone (for dexamethasone) (Yuan *et al.*, 2015). Data were acquired in positive electrospray ionization mode and are shown as % recovery of the stock treatment solutions.

Cisplatin (Pt) analysis was performed in 100 μl effluent samples that were digested by adding 2.4 ml of 1% nitric acid (Millipore Sigma, Burlington, Massachusetts) and shaken to allow any gases to escape. The samples were left overnight to ensure complete digestion. Calibration concentrations ranged from 0 to 300 μM. Blanks containing cell culture media (100 μl) and acid (2.4 ml) were analyzed along with each sample batch. Samples and calibration standards were analyzed on an ICP-Mass Spectrophotometer NexIon 300 (Perkin Elmer, Waltham, Massachusetts). Concentrations were determined as Pt (195), the most abundant isotope, to provide the best sensitivity and were based on a linear calibration curve ($r^2 > 0.99$) using bismuth as an internal standard (Zhang *et al.*, 2016). To avoid carryover, 2% of nitric acid was used as a wash between sample analyses. Results are shown as % recovery from stock treatment solutions.

Determination of drug-free fraction. Rapid equilibrium dialysis (RED) inserts (ThermoFisher, Austin, Texas) were used to determine the free fraction of each test compound in culture media. Solutions (100 μl) of test compounds in cell culture media were placed into the sample chamber, and PBS (350 μl) was added to the buffer chamber. RED plates were incubated at 37°C for 4 h on a rotary shaker at 400 RPM. After incubation, 200 μl of supernatant was collected from each chamber, combined with 200 μl of PBS or cell culture medium (for sample and buffer chambers, respectively), and spiked with the internal standard (10 μl). Samples were extracted by adding 200 μl chilled acetonitrile and centrifuged at 4°C for 10 min at 10 000 g. After separation, the top fraction was collected and concentrated, then reconstituted in LC-MS aqueous phase (acetonitrile with 1% [w/w] formic acid). Samples were analyzed for either LC-MS/MS (linsitinib, doxorubicin, methotrexate, vincristine, and dexamethasone) or ICP-MS (cisplatin) as described above.

Tumor cell viability. The ONE-Glo™ luciferase assay (Promega, Madison, Wisconsin) was used to quantify tumor cell viability in 2-dimensional and 3-dimensional cultures. 3D-B and 3D-B/T scaffolds were cut in half through the center of the tumor, such that the entire cross-section is exposed and can be tested for cell viability. The samples were placed into a standard 96-well plate and treated along with 2-dimensional monolayers with the assay reagent for 10 min in dark. After incubation, a plate reader (BioTek, Winooski, Vermont) was used to measure luminescence. Background signal from bone tissue was removed by subtracting 3D-B values from 3D-B/T readings. Values were shown as percent control (wells or scaffolds treated with the 0.1% DMSO vehicle).

Gene expression profiling. Transcriptome analysis of 2-dimensional and 3-dimensional cultures was conducted using the Templated Oligonucleotide Sequencing Assay (TempO-Seq™, BioSpyder Technologies, Carlsbad, California) using previously established methods (Grimm *et al.*, 2016; House *et al.*, 2017). Cell lysates from plates or 3-dimensional tumors were prepared using the lysis buffer (provided with TempO-seq probes). After 10-min incubation at room temperature, lysates were stored at −80°C until testing. TempO-seq libraries were prepared according to manufacturer's protocols using the ToxPanel targeted transcriptome panel consisting of 2982 transcripts. Briefly, hybridization of the mRNA content was achieved by incubation of 2 μl cell lysate and 2 μl of hybridization mix for 10 min at 70°C, cooling from 70°C to 45°C over 49 min, and incubation at 45°C for 1 min. Excess oligonucleotides were digested at 37°C in a nuclease catalyzed reaction for 90 min. Hybridization products were incubated with DNA ligase (60 min, 37°C), and nuclease and ligase were denatured (30 min incubation, 80°C). About 10 μl of each ligation product

was mixed with 10 µl of PCR amplification mix, and amplified in a LightCycler 96 (Roche, Basel, Switzerland). Amplicon samples (5 µl) were pooled and purified using a commercial PCR clean-up kit (Clontech, Mountain View, California). These pooled libraries were sequenced in 50 single-end read mode using a rapid flow cell on a HiSeq 2500 Ultra High Throughput Sequencing (Illumina, San Diego, California).

Sequencing reads from demultiplexed FASTQ files were aligned using the temposeqcount application (House *et al.*, 2017). Probes with less than 5 counts and samples with less than 100 counts/gene were removed from further analysis. The resulting raw expression count matrix (n = 2, 977 genes) was subsequently normalized, and the differential gene expression analysis was conducted using DESeq2 (Love *et al.*, 2014). Genes were selected for dose-response modeling and point-of-departure estimates were calculated as described in (House *et al.*, 2017). Venn diagrams were constructed using jvenn (Bardou *et al.*, 2014). Reactome ontology sets were paired to occupancy amongst the 2977 probes. Genes in each treatment that passed the QC flags for dose-response modeling (House *et al.*, 2017) were examined for overlap of at least 5 genes in Reactome ontologies. In addition, the Database for Annotation, Visualization and Integrated Discovery (DAVID) v.6.8 (Huang *et al.*, 2009) was used for functional annotation of pathways. Sequencing data are available from Gene Expression Omnibus (GSE135323).

Immuno-histochemistry. Two-dimensional and 3-dimensional tissues were fixed in 10% formalin. The 3-dimensional tissues were embedded in paraffin and sectioned to 4 µm. Fixed wells and tissue sections were stained with hematoxylin and eosin (H/E) to measure the tumor growth area.

Lactate dehydrogenase and osteopontin. Daily supernatant samples from 2-dimensional to 3-dimensional cultures were analyzed to detect lactate dehydrogenase (LDH) using a commercial colorimetric detection kit (Abcam, Cambridge, Massachusetts). TE-B and TE-B/T supernatant samples were tested for Osteopontin (OPN) by a commercial ELISA kit (Abcam). OPN was not measured in 2D-T samples, as these did not contain a "bone" component. All samples were tested following the manufacturer's protocols.

Statistical analyses. All data are presented as mean ± SEM. Statistically significant differences denoted as $p < .05$ were determined using either an unpaired Student's *t* test or a one-way analysis of variance, as indicated in corresponding figure legends.

RESULTS

Bioengineered human bone-tumor model and drug treatments

We utilized human bone tumors that were bioengineered *in vitro* and maintained in culture for prolonged periods of time (weeks to months) (Marturano-Kruik *et al.*, 2016; Villasante *et al.*, 2014). Fully decellularized bovine bone scaffolds (8 × 4 × 1 mm) were first seeded with hMSCs and, after 4 weeks of osteogenic differentiation, infused with ES cell spheroids (3D-B/T), or were cultured without ES spheroids (3D-B). The 3D-B/T and 3D-B models were bioengineered at Columbia University and then shipped overnight to Texas A&M University, where they were cultured for an additional 4–6 weeks in ES medium. In parallel experiments, ES cells were cultured in the same medium in a traditional monolayer culture (2D-T). Three-dimensional and 2-dimensional cultures were exposed to a number of anticancer drugs on designated days, as shown in Figure 1. Medium was replaced daily in all cultures. At the end of each experiment, tumors and cells were fixed or flash frozen for imaging and molecular analyses.

To enable comparisons with the effects of the tested drugs seen clinically in patients, and to characterize the nonspecific binding of drugs in the engineered tissues, we conducted a series of experiments (Figure 2). Rapid equilibrium dialysis was used to characterize free fraction of each drug in the ES cell culture media (Figure 2A). The bioavailability of all compounds was ≥50%. Next, we tested nonspecific binding of drugs in scaffolds, without (Figure 2B) or with (Figure 2C) 3-dimensional tissues. The drugs were present in culture medium only on treatment days. Most of the drug was removed during medium replacement. Doxorubicin demonstrated some binding to the scaffolds materials, as 50–80% of the free fraction was recoverable from the scaffolds without cells. Only linsitinib was lost to a considerable extent (75–40%) in 3-dimensional cultures, a finding consistent with its rapid elimination and extensive biotransformation observed clinically (Poondru *et al.*, 2016).

Reproducibility of the bioengineered human bone-tumor model

Bioengineered ES tumors prepared at Columbia University were tested with linsitinib and doxorubicin using clinically observed concentrations (Figure 3). ES cells grew well in the microphysiological environment and the selected drugs had clear cytotoxic effects. Effects of linsitinib were more pronounced in experiments in laboratory 1, but both laboratories demonstrated similar degrees of drug cytotoxicity. The effects of doxorubicin were nearly identical in the 2 laboratories, with over a 99% reduction in cancer cell viability. Laboratory 2 also tested ES cells in 2-dimensional cultures and showed greater potency compared to that in 3D-B/T model. Interestingly, doxorubicin had a more pronounced effect on the bone compartment of this model (elevated osteopontin), as compared to linsitinib (Supplementary Figure S1), consistent with the evidence of direct bone effects of doxorubicin (Fan *et al.*, 2017).

Another test of the model reproducibility, especially between different batches of the bioengineered human bone tumors, was the confirmation of gene expression profiles. Figure 4 shows that more than one-third of the transcripts interrogated were different between bioengineered bone tumors and bone (Figure 4A). To examine concordance in the transcriptomic signature of this complex model between independent experiments, gene expression profiles of vehicle-treated tissues were compared. Even though tissue constructs were cultured for either 4 weeks (top graph) or 3 weeks (bottom graph), 84% of the transcripts that were significantly different between bone tumors and bone were identical (Figure 4B, top). Moreover, the level of significance in the difference of expression of these transcripts between bone tumors and bone tissue was also highly concordant between 2 time points examined (Figure 4B, bottom). Functional annotation clustering of the overlapping transcripts showed enrichment in a number of classic cancer-related biological process pathways including cell proliferation, DNA damage repair, and apoptosis (Supplementary Table S1).

Assessment of gene expression in drug-treated tumors was not possible because of the significant cell death due to treatments and difficulty of extracting mRNA.

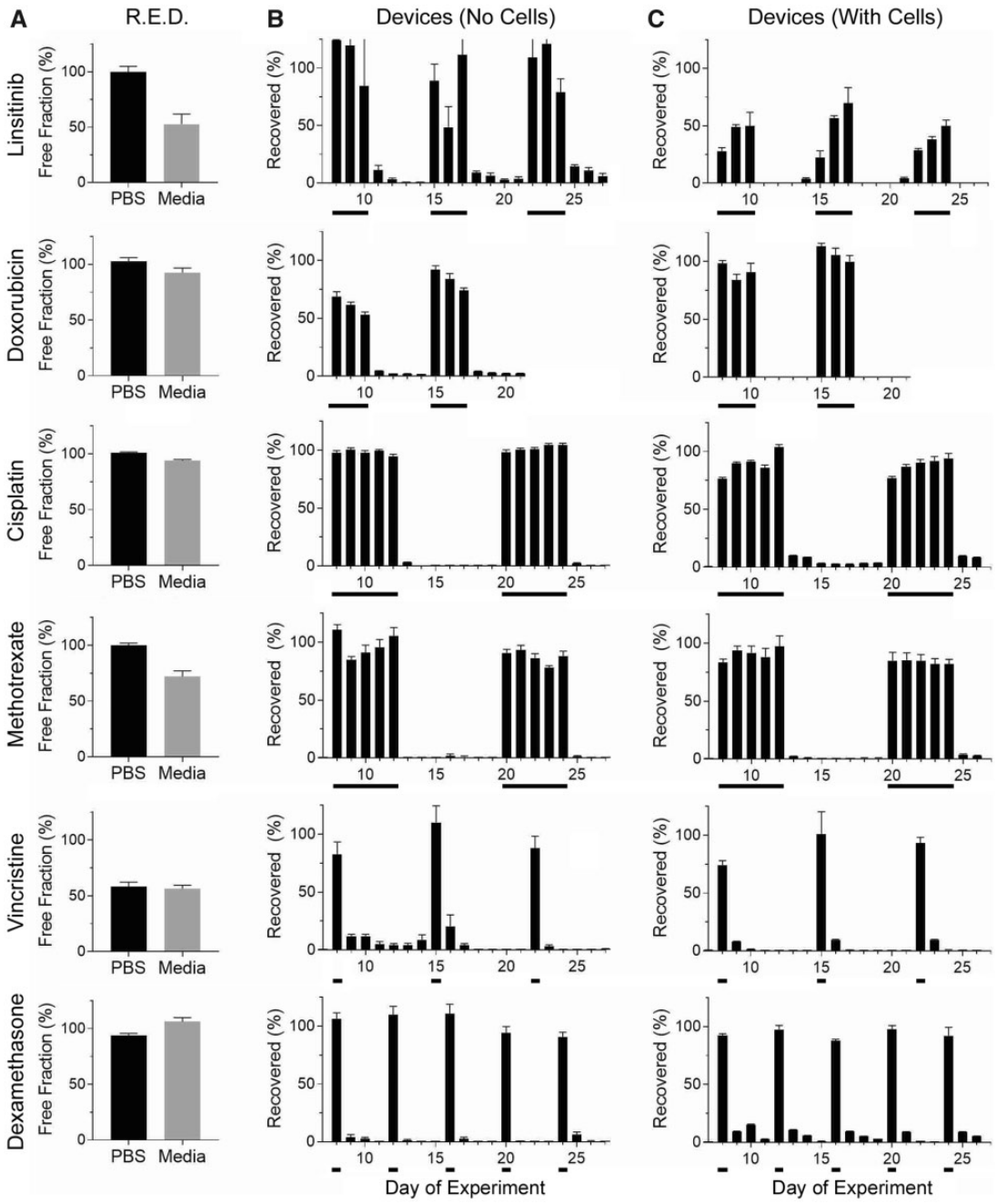

Figure 2. Pharmacokinetic parameters for the drugs and 3-dimensional scaffolds. A, Results of the rapid equilibrium dialysis assay to determine free fraction of each drug in cell culture media. B, Fractions of drugs recovered after 24-h incubation in the scaffolds without cells. C, Fraction of drugs recovered after 24-h incubation in the scaffolds with cells. In B and C, the time-course is shown for the duration of each experiment and the times when the drug was present are indicated by the horizontal bars below each x-axis. Data are expressed as mean ± SEM ($n \geq 3$ replicates). Abbreviation: R.E.D., rapid equilibrium dialysis.

Testing anticancer drug efficacy in the bioengineered human bone tumors

To test the utility of the bioengineered tumor model for drug-efficacy screening, we conducted a series of experiments of chemotherapeutic drugs commonly used for bone tumors (Meyers, 2015), using dexamethasone as a control, as this glucocorticoid has been associated with osteoporosis and osteonecrosis (Weinstein, 2012). Dose-response was evaluated for each of the drugs, and their effects were compared between 3D-B/T and 2D-T models (Figure 5). We evaluated 96 3D-B/T scaffolds simultaneously over an almost 6-week long period (Figure 1B). Drugs were added as specified to simulate clinical treatments, and the ES cell viability was evaluated 2 weeks after the last drug treatment.

Representative H/E-stained images of bone-tumor scaffolds are shown in Figure 5A. The numbers of ES cells were dramatically reduced as compared to drug-free controls, where ES cells filled the spaces between trabeculae. Quantitative analysis of cell viability in 3D-B/T group is shown in Figure 5B. Concentration-dependent ES cell toxicity was evident for all chemotherapeutic agents. Interestingly, dexamethasone also tended to decrease viability of ES cells, while the effect was not

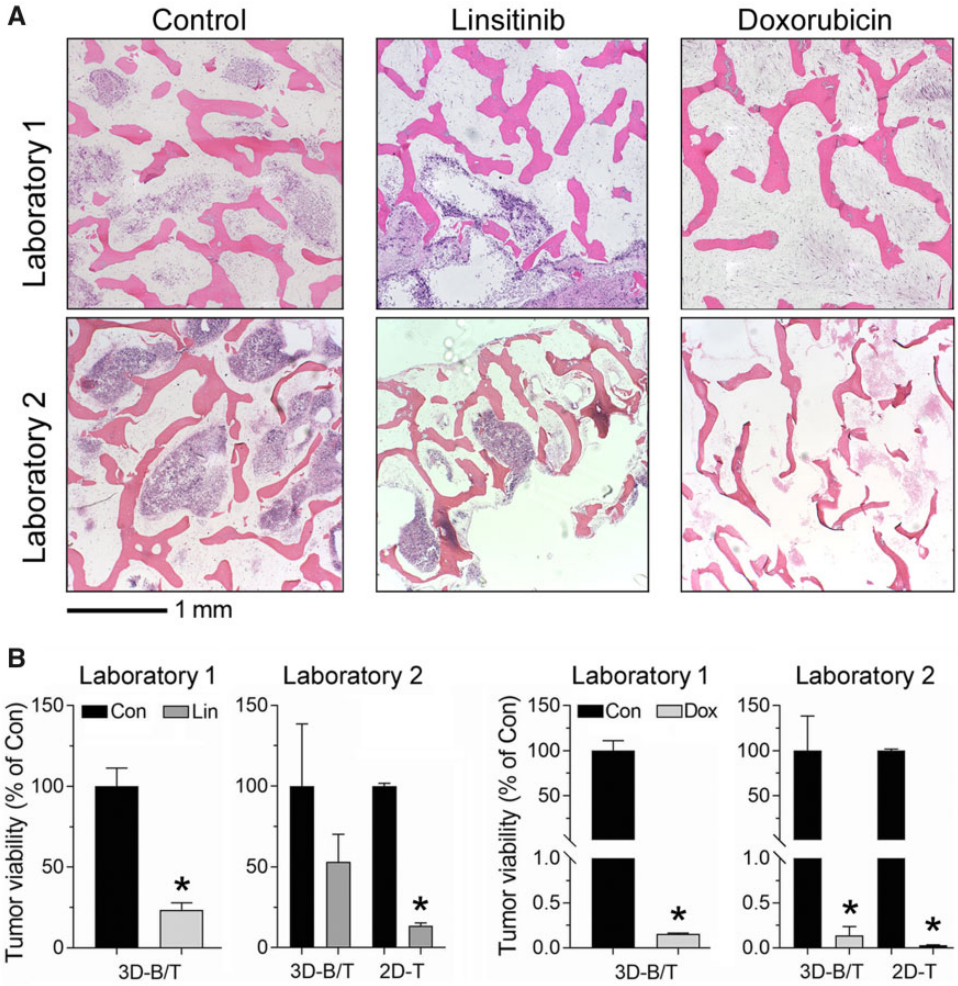

Figure 3. Histopathology and cell viability endpoints demonstrating reproducibility of the results between the 2 laboratories. A, Representative microphotographs of the hematoxylin-eosin-stained sections of 3-dimensional bone-tumor scaffolds treated with vehicle ("Control," 0.1% dimethyl sulfoxide), linsitinib (12 μM), or doxorubicin (4.16 μM). Cell masses indicate tumor cell growth. Contiguous areas represent bone scaffold trabeculae. Data for 2 laboratories are shown separately. B, Tumor (Ewing sarcoma) cell viability on the last day of the experiment after treatment with either linsitinib (left panels) or doxorubicin (right panels) in 3-dimensional bone-tumor and 2-dimensional Ewing sarcoma cell monolayers (in laboratory 2 experiments) are shown relative to vehicle-treated control ("Con") cells. Data are expressed as mean ± SEM ($n \geq 3$ replicates). Asterisks denote significant difference ($p < .05$) between drug-treated and control groups according to an unpaired *t* test. Abbreviations: 2D-T, 2D Ewing sarcoma cell monolayers; 3D-B/T, 3D bone-tumor.

significant. In the 2D-T group (Figure 5C), similar effects were observed, with cisplatin effectively eliminating all cells. Dexamethasone had no effect on ES cell viability in this model, showing that the observed effect in 3D-B/T group was likely due to the adverse effects on mesenchymal cells that impacted the viability of ES cells.

The effects of drugs on bone and ES cells cannot be distinguished in 2-dimensional monolayers but can be achieved using the 3D-B/T model. We monitored the release of osteopontin and LDH into the culture medium over the course of the experiment (Supplementary Figure S2). The treatment with methotrexate, MAP and dexamethasone suppressed osteopontin release, consistent with the known effects of these drugs on osteoclasts (Sun *et al.*, 2014). At the same time, monitoring of LDH in the culture media in either 3-dimensional or 2-dimensional models was less informative, as the levels of LDH decreased because of the loss of live cells, and the spikes in LDH were not detected. Therefore, the utility of this biomarker for continued monitoring of cell viability may be limited.

Effects of drugs used in this study were also assessed through the changes in gene expression. Similar to the experiments with linsitinib and doxorubicin, we were unable to determine gene expression in 3-dimensional tumors due to low viability and difficulty in extracting material. However, robust dose-response effects were observed in the 2-dimensional model (Figure 6). First, we identified differentially expressed genes and calculated the transcriptomic concentration-response points of departure (Figure 6A). We showed dose-dependent effects on expression of *CHEK1*, a key regulator of checkpoint-mediated cell cycle arrest in response to DNA damage.

Across treatments with 5 drugs, all chemotherapeutic agents showed robust responses with hundreds of affected transcripts showing significant dose-response relationships (Figure 6B). Only dexamethasone had little effect on ES cells, as expected. Effects of cisplatin, methotrexate, and MAP, a combination therapy that includes both drugs, were highly overlapping. Vincristine had the most pronounced effect on the transcriptome of ES cells. When dose-response transcriptomic data were

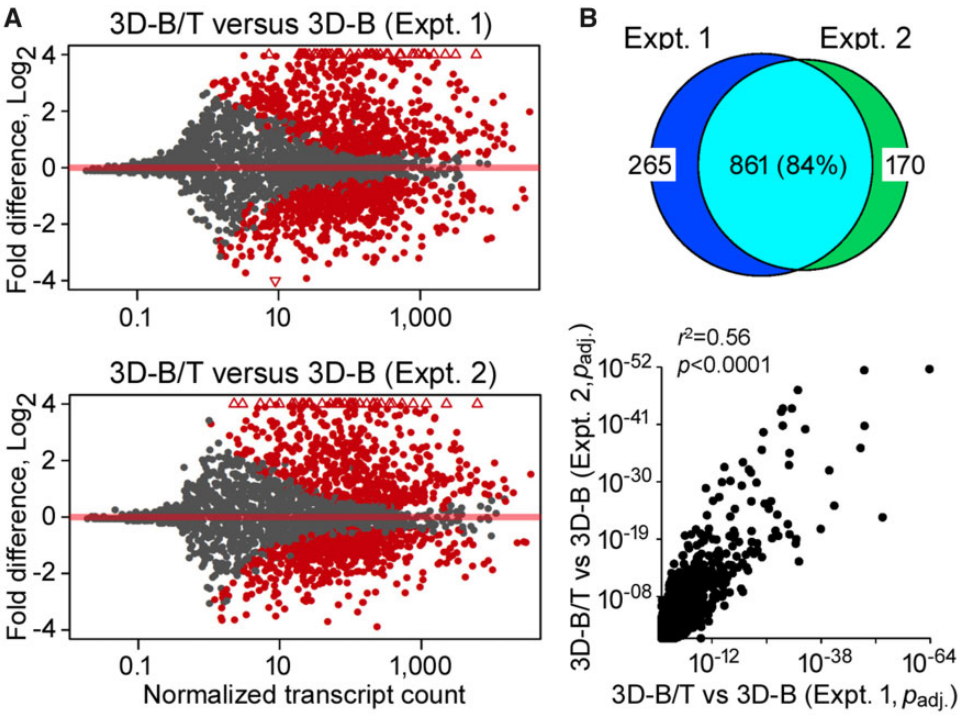

Figure 4. Transcriptome analysis for 3-dimensional scaffolds. A, MA plots depict each transcript in the analysis using the values for "M" ($\log_2$ ratio of the difference between vehicle-treated 3D-B/T and 3D-B samples) and "A" (normalized transcript counts). Two experiments are shown where scaffolds were prepared independently and treated with vehicle (0.1% dimethyl sulfoxide) for either 27 (experiment 1) or 20 (experiment 2) days (see Figure 1A) in the same laboratory. Transcripts that are significantly different ($p_{adj} < .05$ according to pairwise *t* test with Bonferroni correction) are colored as not black. Triangles show transcripts with fold-differences that exceed $|\log_2|=4$. B, Significantly different transcripts identified in experiments shown in Panel A have been compared between experiments. The Venn diagram shows the extent of the overlap in gene lists and the numbers of significant transcripts in each list are shown to the side of both circles. The scatter plot shows p_{adj} values for the transcripts that overlap between 2 experiments. Pearson correlation coefficient (*r*) and the corresponding *p*-value are shown. Abbreviations: 3D-B, 3D bone; 3D-B/T, 3D bone-tumor.

used to derive dose-response pathways (Figure 6C), we observed similar trends. Interestingly, all 4 chemotherapeutic agents shared the majority of the dose-responsive pathways (Figure 6D) and their effects correlated to their cytotoxicity measured by DNA damage and chromatin effects. Vincristine affected a larger number of pathways as compared to other drugs, primarily those governing chromatin remodeling and mitotic arrest, concordant with its known effects on the spindle assembly checkpoint that results in an accumulation of cells in prometaphase (Havas *et al.*, 2016).

Finally, we compared dose-response effects of drugs to the human C_{max} values reported from clinical studies (Figure 7). For all drugs except for cisplatin, we used concentrations that, after correction for free fraction and scaffold binding of each drug (Figure 2), corresponded to human C_{max} values. Effects of drugs on gene expression in the 2-dimensional model were observed at concentrations that were within 1 order of magnitude, but lower than C_{max}, except for cisplatin where they were greater than C_{max}. Pathway-based points of departure were less variable as compared to gene expression-based values at the individual transcript level, regardless of the choice of the median or minimal transcript to calculated pathway dose-response. Interestingly, the points of departure derived from the cell viability measurements were most aligned with the human C_{max} range, especially for the 3D-B/T model. Treatments with dexamethasone had no effect on cell viability in either 2-dimensional or 3-dimensional models and only a minimal effect on gene expression. Pathway analysis of the small number of transcripts affected by dexamethasone treatment yielded no significant findings.

DISCUSSION

A common challenge to the wide adoption of tissue chip models is the perceived complexity of their assembly and maintenance, as well as concerns over the reproducibility of the findings in these complex systems (Ewart *et al.*, 2017; Low and Tagle, 2017). Few examples of successful replication of complex tissue chip models have been published (Sakolish *et al.*, 2018); therefore, one area of emphasis of this study was evaluation of the reproducibility of the bioengineered bone-tumor model.

If bioengineered human bone-tumor models are to be used as a preclinical drug-screening paradigm, the key components of the bone-tumor microenvironment need to be robust, replicable, and have a reasonable throughput. Thus, it is noteworthy that despite the complexity of the model, it was successfully transferred between 2 independent laboratories. In addition, we demonstrated the substantial throughput that allowed for studies of multiple drugs and concentrations in clinically relevant testing regiments with on/off treatment periods spanning multiple weeks that would otherwise not be possible with traditional monolayer culture. To establish the utility of the 3-dimensional tissue models of human tumors, we compared it to the most frequently used study model—a monolayer culture of tumor cells.

The bioengineered tissues provide complex models that more faithfully replicate the complexities of the human tumors in 3-dimensional microenvironment of the bone (Grayson *et al.*, 2010; Marturano-Kruik *et al.*, 2016). Tests of cytotoxic potential of drugs in a monolayer of cancer cells are straightforward, yet the translation of the efficacy and potency of the

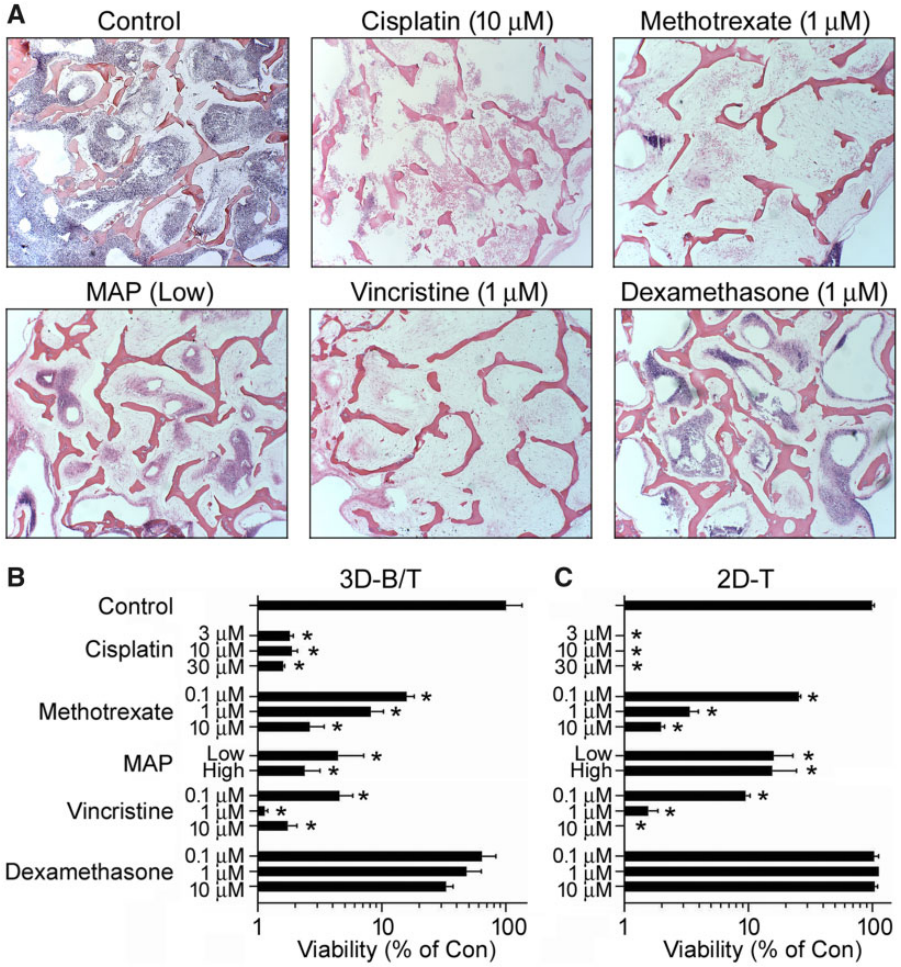

Figure 5. Histopathology and cell viability endpoints for the 3-dimensional and 2-dimensional models. A, Representative microphotographs of the hematoxylin-eosin-stained sections of 3D-B/T scaffolds treated with the vehicle alone ("Control," 0.1% dimethyl sulfoxide), cisplatin (10 μM), methotrexate (1 μM), MAP (low dose), vincristine (1 μM), or dexamethasone (1 μM). B and C, Concentration-dependent effects of the 5 drugs on Ewing sarcoma cell viability in either 3D-B/T (B) or 2D-T (C) models. Effects are shown relative to the vehicle-treated cells. Data are expressed as mean ± SEM ($n \geq 3$ per group and time point). Asterisks denote significant differences in tumor viability between the drug-treated and control groups for each model according to a one-way analysis of variance. Abbreviations: 2D-T, 2D Ewing sarcoma cell monolayers; 3D-B/T, 3D bone-tumor.

chemotherapeutic agents from a dish to *in vivo* is very challenging (Carvalho *et al.*, 2017). In this regard, we show that while it is impossible to recreate the exact tumor microenvironment within the bioengineered bone, the tissue morphology is very similar between 2 testing sites, and therefore, tissues can be successfully transported, remain viable, and undergo few significant changes. Bioengineered bone tumors showed similar ES cell coverage in scaffolds qualitatively before and after treatment, as well as highly concordant gene expression signatures between experiments, demonstrating high expression of tumor-related genes in the bioengineered bone tumor. Doxorubicin's effects in the bioengineered bone-tumor tissues were very similar between labs; however, linsitinib treatment was less potent in laboratory 2. This finding agrees with experimental (Lamhamedi-Cherradi *et al.*, 2016) and clinical (Dutton *et al.*, 2018) data that linsitinib, a dual IGF-1R/insulin receptor alpha inhibitor, is only selectively effective in some patient cohorts.

To fully determine the value of the tissue chip models with respect to their potential as a superior *in vitro* test system, a direct comparison with traditional 2-dimensional models is needed (Carvalho *et al.*, 2017). Therefore, our experiments included a direct comparison of the effects of drugs on a monolayer culture of ES cells. We observed that tumor cells grown in 2-dimensional culture were more sensitive to anticancer drugs. In the bioengineered bone-tumor model, ES cells are grown in spheroids within the bone microenvironment, similar to the pathophysiology of the tumor *in vivo*; thus, higher concentrations are needed to affect tumor cell aggregates. This observation is evidence of the advantages of the bioengineered tissues for drug testing as compared to simplistic 2-dimensional cultures because of the much higher proliferation rate of the cancer cells in a monolayer as compared to a 3-dimensional tissue. In addition, the lower susceptibility of the bioengineered bone-tumor model also exhibits upregulation of key cancer pathways (Villasante *et al.*, 2014), a tumor response that contributes to resistance to treatments *in vivo*.

Another advantage of the complex tissue-like structure is the ability to test drug-tissue/device interactions to better characterize kinetics of the drugs in a realistic tissue microenvironment. Concerns have been voiced with the potential for artifacts from binding of hydrophobic drugs to the exposed surfaces of the scaffolds, depending on their material (Auner *et al.*, 2019). Even though in these experiments the bone-tumor

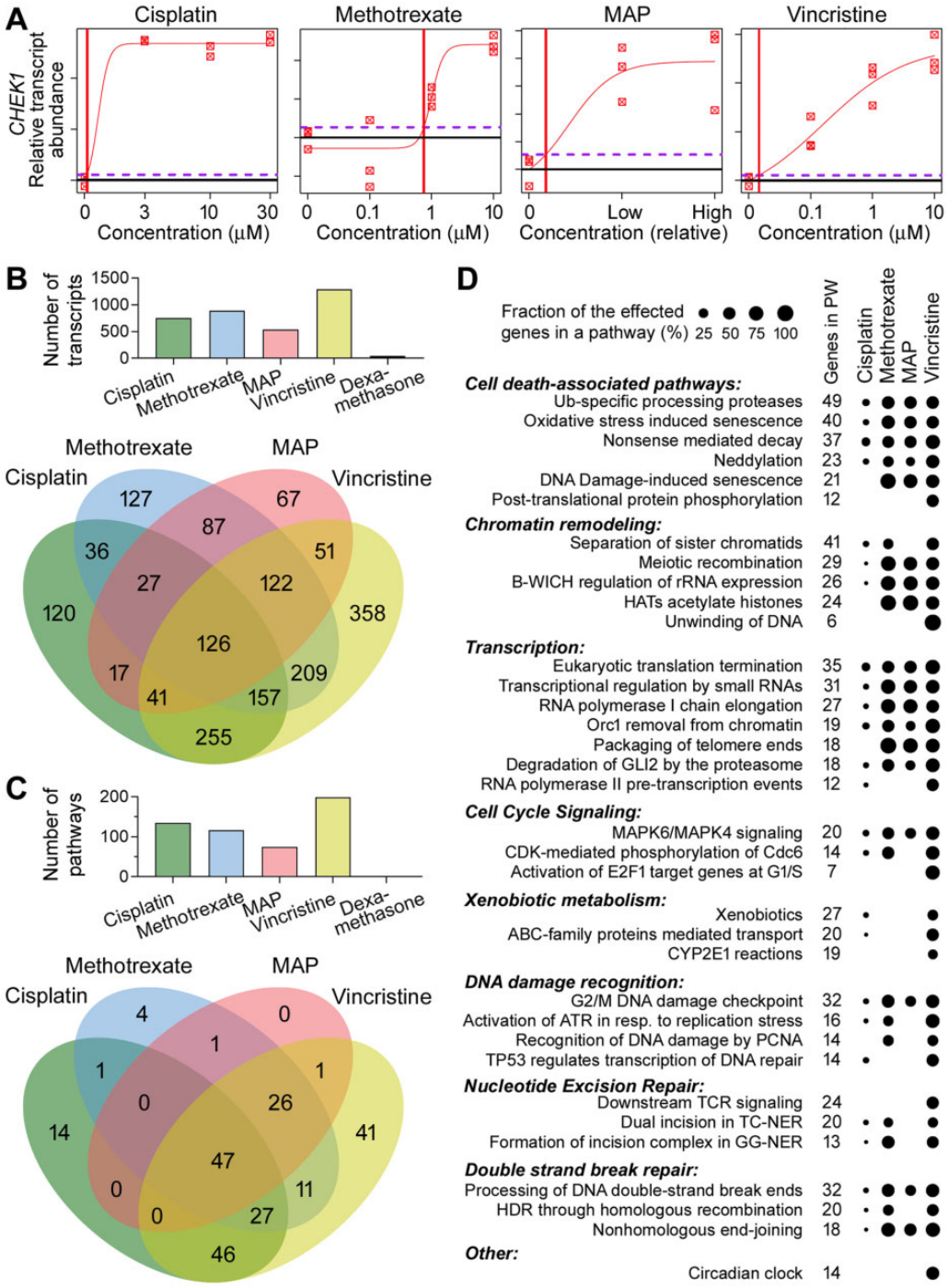

Figure 6. Concentration–response analysis of the transcriptome data for drug effects on Ewing sarcoma cells. A, Example 4-parameter logistic curve fits to the data on *CHEK1* expression after treatment with drugs on day 37 of the experiment (Figure 1B). Before plotting, data were normalized to transcript abundance in wells treated with vehicle alone (0.1% dimethyl sulfoxide). A benchmark response for the point-of-departure in the concentration–response curve (vertical lines) was defined as one standard deviation (horizontal dashed lines) of the mean for vehicle controls (horizontal black lines). Individual replicates are shown. B, The number of transcripts with significant concentration–response relationships (see Materials and Methods) among treatments, and a Venn diagram of their overlap (dexamethasone data were not included due to the low number of significant transcripts) created using jvenn (Bardou *et al.*, 2014). C, The number of significant Reactome pathways identified from the transcripts in Panel B and their overlap (Venn diagram). D, Representative treatment-specific dose-responsive pathways are shown with respect to the overlap among treatments. The number of transcripts in each pathway is shown with the circles depicting the fraction of the effected genes in each pathway.

scaffolds were cultured in polycarbonate plates and not in polydimethylsiloxane (PDMS), binding of the drugs to the plates, to the proteins in the media, and uptake by cells still need to be evaluated. With respect to drug binding to the media proteins, linsitinib and methotrexate were found to have an appreciable degree of binding with 50–75% of the drug remaining as a free fraction. The polycarbonate plates showed some nonspecific binding only for doxorubicin, commensurate with a known affinity of this drug to polycarbonate polymers (Yu *et al.*, 2016). However, in the scaffolds with cells, we found that linsitinib

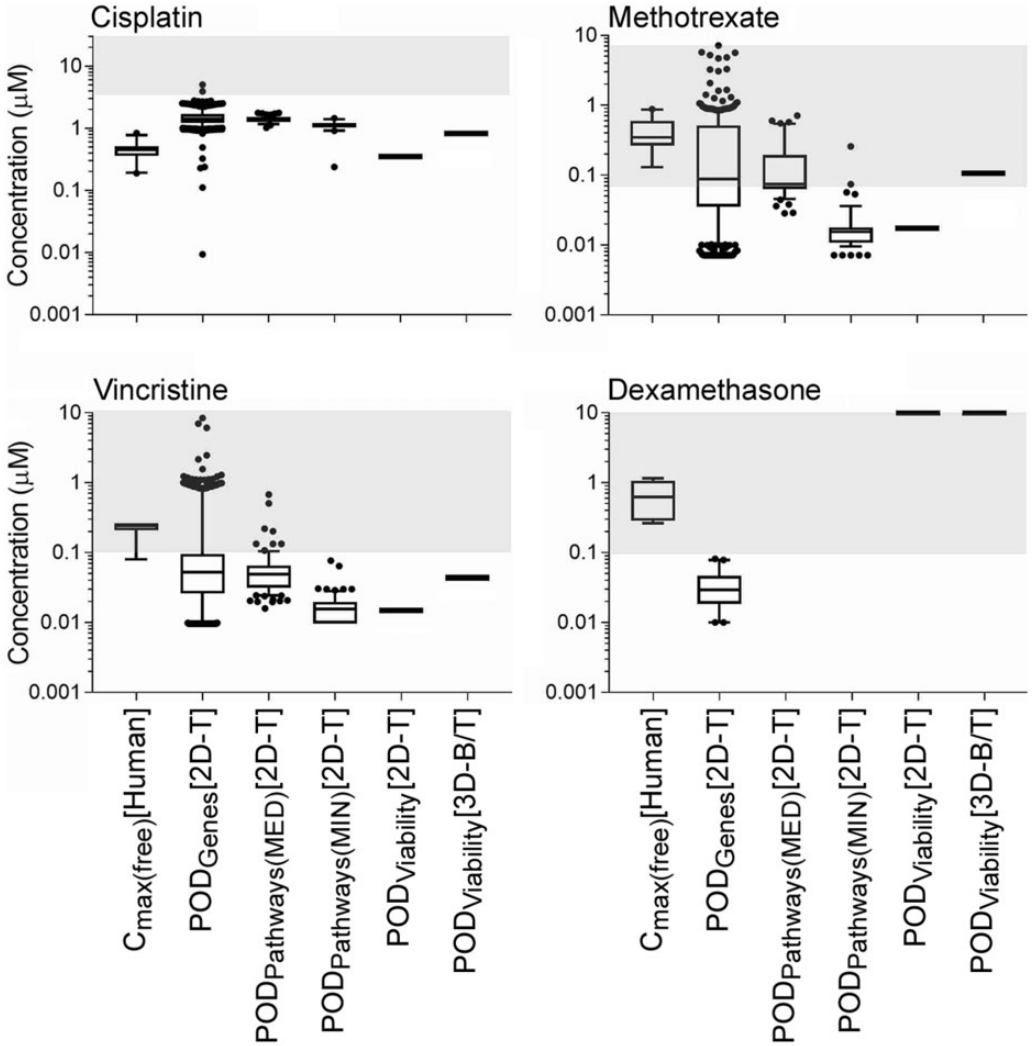

Figure 7. Comparison of the human plasma levels of drugs and their experimentally derived point-of-departure (POD) values in 2D-T and 3D-B/T models. Data for the 4 drugs tested in the experiments detailed in Figure 1B are shown. Gray shading indicates the range of free concentrations of each drug in culture media. Other data are shown as box-and-whiskers plot where the horizontal line is a median value, the box is the interquartile range and the whiskers show 5–95 percentile range. Outlier values are shown as dots on each graph. Human C_{max} values were obtained from Pharmapendium and corrected based on free fraction of drug in human serum. POD_{genes} were calculated using concentration-response data as detailed in Materials and Methods. $POD_{pathways}$ for each pathway represents either the median POD (MED) among the transcripts in that pathway, or the minimum POD (MIN) of a transcript in that pathway. $POD_{viability}$ was calculated from concentration-response data shown in Figure 6B (3D-B/T model) or Figure 6C (2D-T model) as detailed in Materials and Methods. Abbreviations: 2D-T, 2D Ewing sarcoma cell monolayers; 3D-B/T, 3D bone-tumor; POD, point-of-departure.

had considerably lower recovery, meaning that it could be absorbed, or otherwise sequestered, by the tissues. Other tested compounds exhibited similar recovery between blank and cell-seeded scaffolds; therefore, we conclude that there was no scaffold binding, and cells were not sequestering these drugs. Importantly, all compounds washed out quickly on non-treatment days showing no retention of the drug by the scaffolds.

Encouraged by the high reproducibility of this model across laboratories, we aimed to test the utility of the bioengineered bone tumors for testing a larger number of drugs and concentrations. We selected several treatments of bone tumors (Meyers, 2015). Dexamethasone is a glucocorticoid that has been associated with osteoporosis and osteonecrosis (Weinstein, 2012) and it was used here as a drug that may have effects on the bone scaffold, but not on the ES cells. These experiments involved simultaneous handling of 96 bioengineered bone-tumor scaffolds, allowed for testing of 3 concentrations, and replication of the clinically relevant on-off dosing regiments over 6 weeks.

The throughput of this study was comparable to, or even greater than, a mouse xenograft experiment, but it was a human model that recreates tumor-bone microenvironment. Dose-response was evaluated for each drug and their effects were compared to the 2-dimensional cultures. All drugs showed dose-response effects. Cisplatin, vincristine, and MAP were most effective in killing ES cells in both the 3-dimensional and 2-dimensional models. Even though the drugs were more effective in 2-dimensional, we posit that the 3-dimensional model is more relevant for testing efficacy of drug candidates as it presents a more realistic scenario that may demonstrate the potential for tumor relapse, as drugs need to be shown as effective on the aggregates of tumor cells.

When we compared the points of departure for the cytotoxicity effects or used gene expression as a phenotype, the

response of the 3-dimensional model to the cytotoxic effects was closer to the human free C_{max} value for each drug, showing a more realistic estimate of the effective dose from this 3-dimensional model. Gene expression-derived concentration-response data from 2-dimensional experiments were also more informative than traditional cytotoxicity estimates, indicating that transcriptomics is a sensitive biomarker, albeit such experiments would increase the cost and decrease throughput of 2-dimensional models. We found that while dexamethasone was nontoxic in 2-dimensional, in 3-dimensional, there was an effect on the viability of ES cells because it is targeting the bone tissue, indirectly affecting the tumor aggregates. Furthermore, vincristine and methotrexate showed a slight increase in osteopontin, indicating potential adverse effects on the bone tissue, and dexamethasone showed the greatest decrease in osteopontin demonstrating a drop in viability of the osteoblasts in the scaffold. Dexamethasone has been shown to affect bone development in previous studies (Chen *et al.*, 2018). Collectively, these data show the ability of the 3-dimensional model to differentiate between effects on tumor versus bone cells and to establish concentration-response relationships for target and off-target effects.

While the results of this study are encouraging with respect to reproducibility and throughput of the bioengineered bone-tumor model, there are a number of limitations to the use of this model as a complete replacement for drug candidate screening in 2-dimensional cancer cell lines. First, the amount of time needed to establish the model is longer (weeks), as compared to 2-dimensional cultures (days). The throughput is lower, and it is more challenging to image and extract material from the tissue chip. On the other hand, the advantages of the 3-dimensional model are many, such as the presence of tissue-tumor microenvironment and ability to study drug binding and kinetics. The former is the most compelling advantage as it is well-established that tumor cell lines cultured in 2-dimensional quickly downregulate genes involved in cell-cell and cell-ECM interactions (Smalley *et al.*, 2006; Zschenker *et al.*, 2012).

Moving forward, additional studies that provide greater confidence in the robustness of the model's performance in different laboratories should be undertaken, with the elements of the ring-trials used for formal validation of the alternative test methods (Griesinger *et al.*, 2016). Still, we posit that the bioengineered bone-tumor model offers a compelling model system for studies of inter-individual variability in drug sensitivity for both cancer cells and human mesenchymal stem cell-derived osteoblasts. There are multiple subtypes of ES and other bone tumors such as osteosarcomas (Ferguson and Turner, 2018; Yu *et al.*, 2017) and tailoring treatments to be patient-specific can be done in a 3-dimensional bioengineered bone-tumor model, as compared to the mouse xenograft model. In addition, our observations that effects on tumor microenvironment may be also monitored in this 3-dimensional model open the possibilities to introduce more cell types to the scaffolds such as osteoclasts that are native to the bone-tumor milieu, and to test a broader array of drugs specifically targeting the microenvironment. Thus, the model presented here enables a wide variety of applications including anticancer drug testing, disease subtype modeling, and personalized medicine.

SUPPLEMENTARY DATA

Supplementary data are available at *Toxicological Sciences* online.

DECLARATION OF CONFLICTING INTERESTS

The authors declared no potential conflicts of interest with respect to the research, authorship, and/or publication of this article.

FUNDING

National Institutes of Health: National Center for Advancing Translational Sciences (TR001950 to I.R.) and National Institute of Biomedical Imaging and Bioengineering (EB0025765 to G.V.N.).

REFERENCES

Abdel-Hamid, M., and Sharma, D. (2004). Simultaneous quantification of doxorubicin, lorazepam, metoclopramide, ondansetron, and ranitidine in mixtures by liquid chromatography-tandem mass spectrometry. *J. Liq. Chromatogr. Relat. Technol.* **27**, 641–660.

Auner, A. W., Tasneem, K. M., Markov, D. A., McCawley, L. J., and Hutson, M. S. (2019). Chemical-PDMS binding kinetics and implications for bioavailability in microfluidic devices. *Lab. Chip* **19**, 864–874.

Bardou, P., Mariette, J., Escudie, F., Djemiel, C., and Klopp, C. (2014). jvenn: An interactive Venn diagram viewer. *BMC Bioinformatics* **15**, 293.

Carvalho, M. R., Lima, D., Reis, R. L., Oliveira, J. M., and Correlo, V. M. (2017). Anti-cancer drug validation: The contribution of tissue engineered models. *Stem Cell Rev.* **13**, 347–363.

Chen, Z., Zhao, X., Li, Y., Zhang, R., Nie, Z., Cheng, X., Zhang, X., and Wang, H. (2018). Course-, dose-, and stage-dependent toxic effects of prenatal dexamethasone exposure on long bone development in fetal mice. *Toxicol. Appl. Pharmacol.* **351**, 12–20.

Chramiec, A., and Vunjak-Novakovic, G. (2019). Tissue engineered models of healthy and malignant human bone marrow. *Adv. Drug Deliv. Rev.* **140**, 78–92.

Dutton, P., Love, S. B., Billingham, L., and Hassan, A. B. (2018). Analysis of phase II methodologies for single-arm clinical trials with multiple endpoints in rare cancers: An example in Ewing's sarcoma. *Stat. Methods Med. Res.* **27**, 1451–1463.

Ewart, L., Fabre, K., Chakilam, A., Dragan, Y., Duignan, D. B., Eswaraka, J., Gan, J., Guzzie-Peck, P., Otieno, M., Jeong, C. G., *et al.* (2017). Navigating tissue chips from development to dissemination: A pharmaceutical industry perspective. *Exp. Biol. Med. (Maywood)* **242**, 1579–1585.

Fan, C., Georgiou, K. R., Morris, H. A., McKinnon, R. A., Keefe, D. M. K., Howe, P. R., and Xian, C. J. (2017). Combination breast cancer chemotherapy with doxorubicin and cyclophosphamide damages bone and bone marrow in a female rat model. *Breast Cancer Res. Treat.* **165**, 41–51.

Ferguson, J. L., and Turner, S. P. (2018). Bone cancer: Diagnosis and treatment principles. *Am. Fam. Physician* **98**, 205–213.

Grayson, W. L., Frohlich, M., Yeager, K., Bhumiratana, S., Chan, M. E., Cannizzaro, C., Wan, L. Q., Liu, X. S., Guo, X. E., and Vunjak-Novakovic, G. (2010). Engineering anatomically shaped human bone grafts. *Proc. Natl. Acad. Sci. U.S.A.* **107**, 3299–3304.

Griesinger, C., Desprez, B., Coecke, S., Casey, W., and Zuang, V. (2016). Validation of alternative *in vitro* methods to animal testing: Concepts, challenges, processes and tools. *Adv. Exp. Med. Biol.* **856**, 65–132.

Grimm, F. A., Iwata, Y., Sirenko, O., Chappell, G. A., Wright, F. A., Reif, D. M., Braisted, J., Gerhold, D. L., Yeakley, J. M., Shepard,

P., *et al.* (2016). A chemical-biological similarity-based grouping of complex substances as a prototype approach for evaluating chemical alternatives. *Green Chem.* **18**, 4407–4419.

Guilhaumou, R., Solas, C., Rome, A., Giocanti, M., Andre, N., and Lacarelle, B. (2010). Validation of an electrospray ionization LC/MS/MS method for quantitative analysis of vincristine in human plasma samples. *J. Chromatogr. B Analyt. Technol. Biomed. Life Sci.* **878**, 423–427.

Havas, A. P., Rodrigues, K. B., Bhakta, A., Demirjian, J. A., Hahn, S., Tran, J., Scavello, M., Tula-Sanchez, A. A., Zeng, Y., Schmelz, M., *et al.* (2016). Belinostat and vincristine demonstrate mutually synergistic cytotoxicity associated with mitotic arrest and inhibition of polyploidy in a preclinical model of aggressive diffuse large B cell lymphoma. *Cancer Biol. Ther.* **17**, 1240–1252.

House, J. S., Grimm, F. A., Jima, D. D., Zhou, Y. H., Rusyn, I., and Wright, F. A. (2017). A pipeline for high throughput concentration response modeling of gene expression for toxicogenomics. *Front. Genet.* **8**, 168.

Huang, D. W., Sherman, B. T., and Lempicki, R. A. (2009). Systematic and integrative analysis of large gene lists using DAVID bioinformatics resources. *Nat. Protoc.* **4**, 44–57. (Research Support, N.I.H., Extramural).

Jacques, C., Renema, N., Lezot, F., Ory, B., Walkley, C. R., Grigoriadis, A. E., and Heymann, D. (2018). Small animal models for the study of bone sarcoma pathogenesis: Characteristics, therapeutic interests and limitations. *J. Bone Oncol.* **12**, 7–13.

Jacques, C., Renema, N., Ory, B., Walkley, C. R., Grigoriadis, A. E., and Heymann, D. (2019). Murine models of bone sarcomas. *Methods Mol. Biol.* **1914**, 331–342.

Khanna, N., Pandey, A., and Bajpai, J. (2017). Metastatic Ewing's sarcoma: Revisiting the "Evidence on the Fence". *Indian J. Med. Paediatr. Oncol.* **38**, 173–181.

Lamhamedi-Cherradi, S. E., Menegaz, B. A., Ramamoorthy, V., Vishwamitra, D., Wang, Y., Maywald, R. L., Buford, A. S., Fokt, I., Skora, S., Wang, J., *et al.* (2016). IGF-1R and mTOR blockade: Novel resistance mechanisms and synergistic drug combinations for Ewing sarcoma. *J. Natl. Cancer Inst.* **108**, 1–12.

Love, M. I., Huber, W., and Anders, S. (2014). Moderated estimation of fold change and dispersion for RNA-seq data with DESeq2. *Genome Biol.* **15**, 550.

Low, L. A., and Tagle, D. A. (2017). Organs-on-chips: Progress, challenges, and future directions. *Exp. Biol. Med. (Maywood)* **242**, 1573–1578.

Marcos-Campos, I., Marolt, D., Petridis, P., Bhumiratana, S., Schmidt, D., and Vunjak-Novakovic, G. (2012). Bone scaffold architecture modulates the development of mineralized bone matrix by human embryonic stem cells. *Biomaterials* **33**, 8329–8342.

Marturano-Kruik, A., Villasante, A., and Vunjak-Novakovic, G. (2016). Bioengineered models of solid human tumors for cancer research. *Methods Mol. Biol.* **1502**, 203–211.

Marturano-Kruik, A., Yeager, K., Bach, D., Villasante, A., Cimetta, E., and Vunjak-Novakovic, G. (2015). Mimicking biophysical stimuli within bone tumor microenvironment. *Conf. Proc. IEEE Eng. Med. Biol. Soc.* **2015**, 3561–3564.

Marx, U., Andersson, T. B., Bahinski, A., Beilmann, M., Beken, S., Cassee, F. R., Cirit, M., Daneshian, M., Fitzpatrick, S., Frey, O., *et al.* (2016). Biology-inspired microphysiological system approaches to solve the prediction dilemma of substance testing. *ALTEX* **33**, 272–321.

Meyers, P. A. (2015). Systemic therapy for osteosarcoma and Ewing sarcoma. *Am. Soc. Clin. Oncol. Educ. Book*, **35**, e644–e647. doi:10.14694/EdBook_AM.2015.35.e644.

Moore, D. D., and Haydon, R. C. (2014). Ewing's sarcoma of bone. *Cancer Treat Res.* **162**, 93–115.

Poondru, S., Chaves, J., Yuen, G., Parker, B., Conklin, E., Singh, M., Nagata, M., and Gill, S. (2016). Mass balance, pharmacokinetics, and metabolism of linsitinib in cancer patients. *Cancer Chemother. Pharmacol.* **77**, 829–837.

Rodin, I., Braun, A., Stavrianidi, A., and Shpigun, O. (2013). A validated LC-MS/MS method for rapid determination of methotrexate in human saliva and its application to an excretion evaluation study. *J. Chromatogr. B Analyt. Technol. Biomed. Life Sci.* **937**, 1–6.

Ronaldson-Bouchard, K., and Vunjak-Novakovic, G. (2018). Organs-on-a-chip: A fast track for engineered human tissues in drug development. *Cell Stem Cell* **22**, 310–324.

Sakolish, C., Weber, E. J., Kelly, E. J., Himmelfarb, J., Mouneimne, R., Grimm, F. A., House, J. S., Wade, T., Han, A., Chiu, W. A., *et al.* (2018). Technology transfer of the microphysiological systems: A case study of the human proximal tubule tissue chip. *Sci. Rep.* **8**, 14882.

Smalley, K. S., Lioni, M., and Herlyn, M. (2006). Life isn't flat: Taking cancer biology to the next dimension. *In Vitro Cell. Dev. Biol. Anim.* **42**, 242–247.

Sun, Y., Yao, Y., and Ding, C. Z. (2014). A combination of sinomenine and methotrexate reduces joint damage of collagen induced arthritis in rats by modulating osteoclast-related cytokines. *Int. Immunopharmacol.* **18**, 135–141.

Villasante, A., Marturano-Kruik, A., Robinson, S. T., Liu, Z., Guo, X. E., and Vunjak-Novakovic, G. (2017). Tissue-engineered model of human osteolytic bone tumor. *Tissue Eng. Part C Methods* **23**, 98–107.

Villasante, A., Marturano-Kruik, A., and Vunjak-Novakovic, G. (2014). Bioengineered human tumor within a bone niche. *Biomaterials* **35**, 5785–5794.

Weinstein, R. S. (2012). Glucocorticoid-induced osteonecrosis. *Endocrine* **41**, 183–190.

Yu, H., Ge, Y., Guo, L., and Huang, L. (2017). Potential approaches to the treatment of Ewing's sarcoma. *Oncotarget* **8**, 5523–5539.

Yu, L., Lin, C., Zheng, Z., Li, Z., and Wang, X. (2016). Self-assembly of pH-responsive biodegradable mixed micelles based on anionic and cationic polycarbonates for doxorubicin delivery. *Colloids Surf. B Biointerfaces* **145**, 392–400.

Yuan, Y., Zhou, X., Li, J., Ye, S., Ji, X., Li, L., Zhou, T., and Lu, W. (2015). Development and validation of a highly sensitive LC-MS/MS method for the determination of dexamethasone in nude mice plasma and its application to a pharmacokinetic study. *Biomed. Chromatogr.* **29**, 578–583.

Zhang, T., Cai, S., Forrest, W. C., Mohr, E., Yang, Q., and Forrest, M. L. (2016). Development and validation of an inductively coupled plasma mass spectrometry (ICP-MS) method for quantitative analysis of platinum in plasma, urine, and tissues. *Appl. Spectrosc.* **70**, 1529–1536.

Zschenker, O., Streichert, T., Hehlgans, S., and Cordes, N. (2012). Genome-wide gene expression analysis in cancer cells reveals 3D growth to affect ECM and processes associated with cell adhesion but not DNA repair. *PLoS One* **7**, e34279.